Microsyst Technol
DOI 10.1007/s00542-014-2399-x

TECHNICAL PAPER

Automated and low cost method to manufacture addressable solid-state nanopores

Milena Vega · Betiana Lerner · Carlos A. Lasorsa · Karina Pierpauli · Maximiliano S. Perez

Received: 14 October 2014 / Accepted: 9 December 2014
© Springer-Verlag Berlin Heidelberg 2014

Abstract In this paper an easy, reproducible and inexpensive technique for the production of solid state nanopores, using silicon wafer substrate is proposed. The technique is based on control of pore formation, by neutralization etchant (KOH) with a strong acid. Thus, a local neutralization is produced around the nanopore, which stops the silicon etching. The etching process was performed with 7 M KOH at 80 °C, where 1.23 µm/min etchings speed was obtained, similar to those published in literature. The control of the pore formation with the braking acid method was done using 12 M HCl and different extreme conditions: (1) at 25 °C, (2) at 80 °C and (3) at 80 °C applying a potential. In these studies, it was found that nanopores can be obtained automatically, addressable and at a low cost. Additionally, a way to obtain the nanopores leaving the silicon wafer completely clean after the etching process was found. This method offers the possibility of an efficient scale-up from the laboratory to production scale.

M. Vega · B. Lerner (✉) · C. A. Lasorsa · M. S. Perez
Special Coating by Plasma Processing Techniques Lab., National Technological University, Buenos Aires, Argentina
e-mail: blerner@frh.utn.edu.ar

M. S. Perez
e-mail: mperez@frh.utn.edu.ar

M. Vega · B. Lerner · M. S. Perez
Biochemical Engineering Group, Buenos Aires University, Buenos Aires, Argentina

B. Lerner · M. S. Perez
Institute of Technological Development for the Chemical Industry, Santa Fe, Argentina

C. A. Lasorsa · K. Pierpauli
Micro and Nanotechnology Group, National Atomic Energy Commission, Buenos Aires, Argentina

1 Introduction

At present, the development of new manufacturing methods for nanopores production is addressing a wide range of investigations. These developments are directed to the production of biological nanopores (Bashir 2011), where the pore is formed by nuclear or membrane bacteria proteins and solid-state nanopores (Edel and Albrecht 2013), which have become an alternative to biological nanopores. This is because they have greater stability, durability, besides being compatible with lithography processes, among other advantages. And finally, hybrid nanopores, where the benefit of biological and solid state nanopores are combined to perform the biomolecules sensing (Hall et al. 2010). The use of nanopores for sensing process is applied to DNA molecules (Fologea et al. 2007; Gierhart et al. 2008; Haque et al. 2013), to other detection as enzyme activities (Fennouri et al. 2012), polypeptides detection (Movileanu 2008), proteins (Rosen et al. 2014) or nanoparticles (Li and Fan 2013), among others. Generally the methodology to fabricate solid state nanopores is a polymer of solid material or a floating membrane supported on a silicon frame. Some examples of materials used as membranes are silicon dioxide and silicon nitride. Due to the potential of the nanopores in a large number of applications, there is continuing interest in the development of new nanopores devices. There is great progress in manufacturing technology of solid-state nanopores in silicon. Using electrochemical etching combined with an electric control of pore opening (Park et al. 2007) nanopores can be obtained. However, this method requires human intervention or a robot to stop etching reaction.

Solid-state nanopores are also produced by other methods like focused ion beam (FIB) (Lanyon et al. 2007; Schiedt et al. 2010) or electron-beam (E-beam) (Rhee and

Published online: 21 December 2014

Burns 2007), but these methods require expensive equipment, and are hardly scalable to produce large quantities. To implement the nanopores in commercial devices, a manufacturing process which is scalable is needed. Therefore it is necessary to have a reproducible manufacturing method that does not require expensive equipment, easy to implement and that presents low costs of production. It is also important that the process allows the manufacture of a nanopore or an array of them in specific locations of the substrate, compatible with other microfabrication processes such as lithography for electrode deposition and/or union with microchannels for fluid injection.

This paper describes a nanopores manufacture method, which solves above mentioned requirements. The method uses an automatic braking pore formation, without the intervention of an external agent, when this has dimensions of 4 nm to 200 μm.

The manufacturing method is based on the chemical braking of etching in silicon wafers for produce solid state nanopores. Nanopores were manufactured using a KOH etching and subsequently a chemical braking was performed with HCl, in order to automatically control the nanopore opening. The neutralizes braking etchant as soon as the chemical pierces the sample, thus interrupting the pore growth.

2 Materials and methods

2.1 Pattern formation

A schematic picture of the pattern forming process is shown in Fig. 1. The substrates used were 700 μm thick double-side polished <100> oriented silicon wafers (Virginia Semiconductor In). Silicon nitride layer of 50 nm thickness were deposited on a wafer using Plasma Enhanced chemical vapor deposition (PECVD) at 600 °C. The gas used for plasma deposition was hexamethyldisilazane $(CH_3)_3SiNHSi(CH_3)_3$ and nitrogen as reactive gas. Square shapes were performed by photolithography using AZ9260 photoresin with a dark-field mask. The photoresin deposit on the silicon wafers was conducted with Spinner at 2,400 rpm, then a pre-heating was conducted for about 3 min at 110 °C, and wetting for 18 min. The photoresin was exposed 40 s using an EVG 620 mask aligner (300 W UV Plane focus light of 6 in. diameter), and developed using AZ 400 developer: DI water 1:4. Subsequently attack by reactive ion etching (RIE) on the wafer both sides was performed. Thus, it is possible to remove the Si_3N_4 layer, exposing the square shapes previously performed on the silicon wafer. The RIE etching process for the Si_3N_4 passivation layer, was carried out in a plasma etching equipment (Plasma lab 80, Oxford).

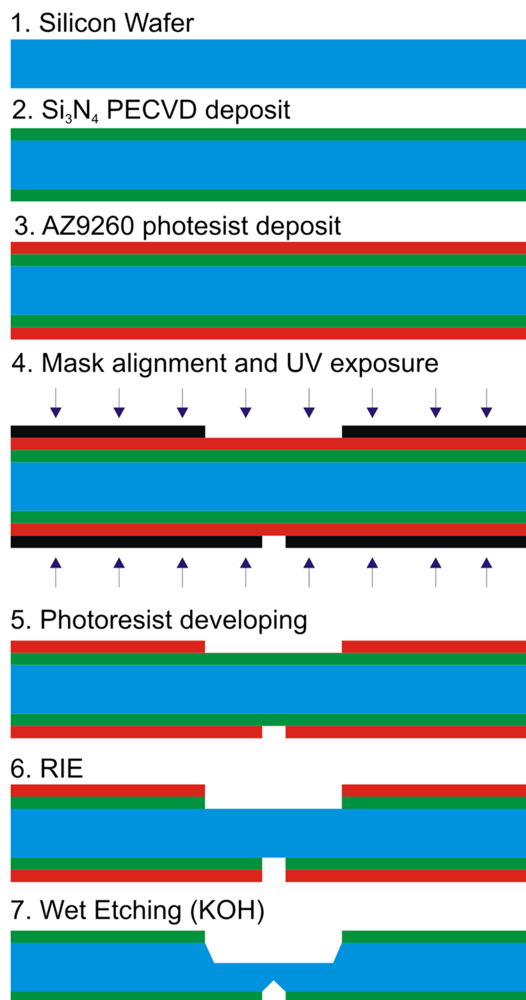

Fig. 1 Steps for the manufacturing process of nanopores on a silicon wafer

The main parameters for the RIE process are the gas mixture, the RF power applied was 13.6 MHz, and the chamber pressure. Subsequently a wet removal of the photoresin is performed with acetone. Figures formed on both wafer faces were aligned so that the resulting squares are concentric.

2.2 Chemical etching

The chemical anisotropic etching of silicon wafers was carried out using KOH 7 M at 80 °C. First, the etching was performed simultaneously on both sides of the silicon wafer. The reaction was stopped before the inverted pyramids formed joined. Subsequently, the silicon wafer was removed from the container in which the first etching was performed. This was washed with deionized water and then, it was introduced into a PDMS device, which is made out a second etching (chemical braking).

The wafer was deposited on a PDMS device between two isolated compartments for carrying out a second etching with 4 M KOH in one side (*cis*), while the opposite side was exposed to HCl 12 M (*trans*). Thus, the etching continues only in one side of the substrate. With the etching advance, the inverted pyramid exposed to KOH grows to the point of meeting the inverted pyramid formed on the opposite side.

The pore size was adjusted by controlling the reaction temperature and/or applying an electrical potential, 15 samples were studied for each condition. Chemical braking was performed at two temperatures: 25 and 80 °C. These two temperatures were chosen to study the process, first at 25 °C and subsequently the temperature according to previous studies (Lerner et al. 2012) where the greater rate of nanopores formation was obtained. A potential of 12 V was also applied to control the reaction rate. For this stage KOH 4 M and HCl 12 M were used, being a simple neutralization reaction, where the HCl is used in excess to ensure the OH^- neutralization. Therefore, a local neutralizing around nanopore occurs, which stops the etching process. However neutralization is low in the dissolution context, because the solution drift through the nanopore is not quantitatively significant, due to the nanopore small diameter.

3 Results and discussion

3.1 Nanopores manufacture by the acid and potential method

The main step in the nanopores formation is the second etching. Thus, the inverted pyramid finish in fine tips joined forming the nanopores. Figure 2 corresponds to the design of the mask used, in which square made of 2.1 mm to form a large window in one side of the wafer, and squares of 270 μm to form pyramids inverted ending in fine tips, on the opposite side of the wafer.

3.2 First etching

As mentioned on Sect. 2.2, a first chemical etching with 7 M KOH at 80 °C for 7 h on both sides of the silicon wafer is performed according to Fig. 3.

This concentration and temperature were selected because together, they generate silicon etching quickly. Etch rate increased because $Si(OH)_2$ heating excites electrons from the 3 s orbital, which pass to the conduction band. In this situation, two electrons are lost and the formation of $Si(OH)_4$ is induced. 4 electrons in total are lost from Silicon valence level, they react with water protons and hydrogen will reduce. The reaction of silicon etching, wherein OH^- ions dissolved silicon, is shown in reaction 1:

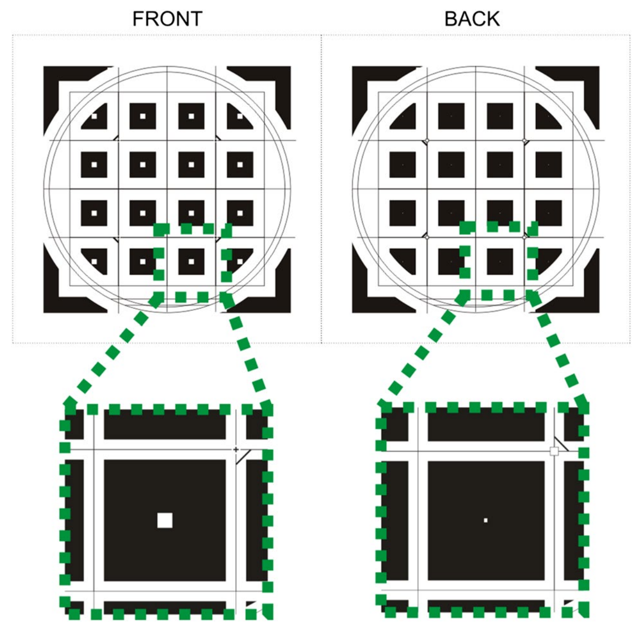

Fig. 2 Mask design for both sides of the wafer, corresponding to inverted pyramids to nanopores form

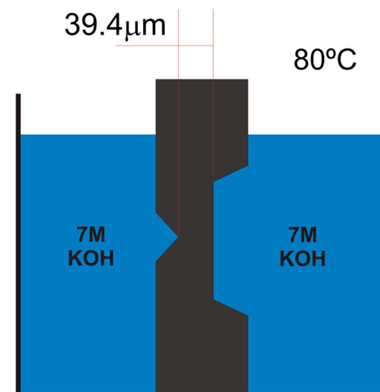

Fig. 3 Silicon nanopores fabrication with chemical braking. Schematic image of the experimental setup (KOH etching)

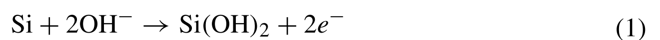

$$Si + 2OH^- \rightarrow Si(OH)_2 + 2e^- \quad (1)$$

Therefore, these 2 electrons are the last two 3p electrons of the valence shell. In this reaction the silicon has been transformed from Si to Si^{2+}, as metal has been oxidized. These two lost electrons, forming a conduction band, and thus, are located offshore (not belonging to any atom) on the element structure surface of the conduction band, in the same way as occurs in metals. The following electrons, which can be lost are the $3s^2$, which lead to silicon valence 4^+ (reaction 2):

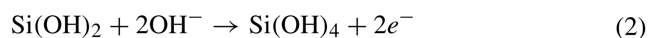

$$Si(OH)_2 + 2OH^- \rightarrow Si(OH)_4 + 2e^- \quad (2)$$

Thus, they lose two other electrons from the valence shell Silicon and also passed to the conduction band, increasing conductivity (power transmission) of the substrate. Thus, the silicon becomes Si^{4+} because is further oxidized. This may be due to the mechanism of the second chemical reaction which occurs by complex formation of $Si(OH)_4$. So, silicon hydroxide (II), by heating, loses the remaining 2 electrons 3s because they are thermally excited and passed to the conduction band. Thus, this complex easily reacts with OH^- present and form silicon hydroxide (IV). 4 electrons lost in total, from the silicon, react with the protons of water and which are reduced to hydrogen. The reaction can be understood as a dissociation of water and reduction of dissociated protons, with formation of molecular hydrogen, According to reaction 3:

$$4H_2O \Leftrightarrow 4H^+ + 4OH^- \quad 4H^+ + 4e^- \rightarrow 2H_2 \tag{3}$$

When protons are reduced form H_2, the chemical equilibrium is totally shifted to the right and then the reaction is defined as (reaction 4):

$$4H_2O + 4e^- \rightarrow 2H_2 + 4OH^- \tag{4}$$

Part of these OH^- generated in reaction 4 stabilized silicon hydroxide (IV), unstable compound, according to reaction 5:

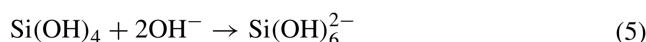

$$Si(OH)_4 + 2OH^- \rightarrow Si(OH)_6^{2-} \tag{5}$$

Where the latter complex is more stable in solution. Etching depths were measured by optical microscopy, recording a depth of 470 ± 2 µm for the window and 191 ± 2 µm for the inverted pyramid. Adding the two depths cavities, total depth is 661 ± 4 µm. To form nanopores in silicon wafer, that after the first etching has a thin thickness of about 39.4 µm, it is necessary to make a second etching. In the second etching, the process is interrupted by the HCl instantly when the nanopore is formed. Therefore, it is possible to automatically control the braking reaction, and this is the key step in the manufacture of the nanopores.

Then, the three processes studied are detailed to carry out the second etching, to evaluate the effectiveness of the technique proposed in this paper.

3.3 Second etching (chemical braking)

3.3.1 Nanopores formation at 25 °C

The chemical braking was performed by introducing the silicon wafer previously attacked with KOH at 80 °C (first etching), in a PMDS device between two compartments isolated for performing a second etching with KOH 4 M in cis face, while the trans side was exposed to HCl 12 M at 25 °C. Thus, the attack continued only on the cis side of the substrate, according to Fig. 4.

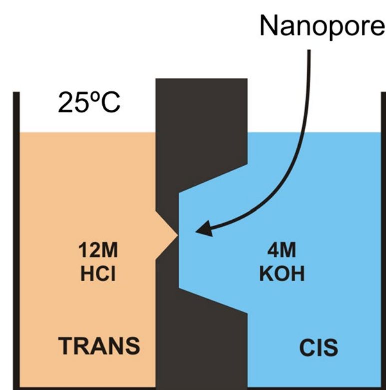

Fig. 4 Second etching process at 25 °C

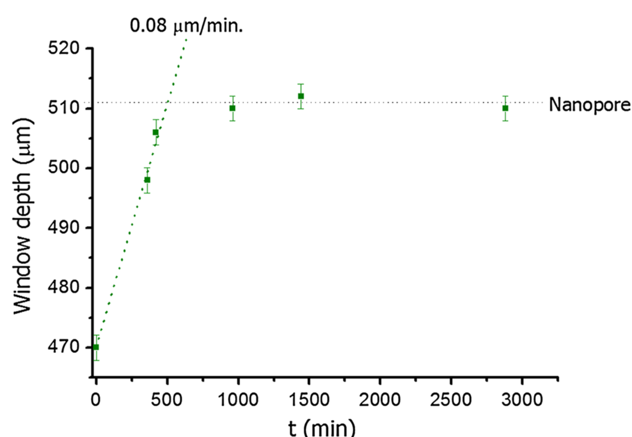

Fig. 5 Window depth of 2.1 mm, depending on the etching time with 4 M KOH at 25 °C

Figure 5 shows the etching rate in the early hours with a speed of 0.083 µm/min, and when the depth of the window reaches 512 µm, the etching is completely stopped, even after 50 h etching.

Thus, it was found that the nanopores are produced after about 8 h of chemical braking, and the process is able to control its formation, up to 50 h of etching later. Formation of nanopores was confirmed by SEM and resistance measurement. Figure 6 shows a nanopore obtained by this technique. Thus, HCl protons have more time to traverse the nanopore newly formed and neutralize the KOH. So, the etching stops and allows the nanopore formation.

3.3.2 Nanopores formation at 80 °C

To evaluate the effect of high temperature on the chemical process of braking, the same process carried out at 25 °C

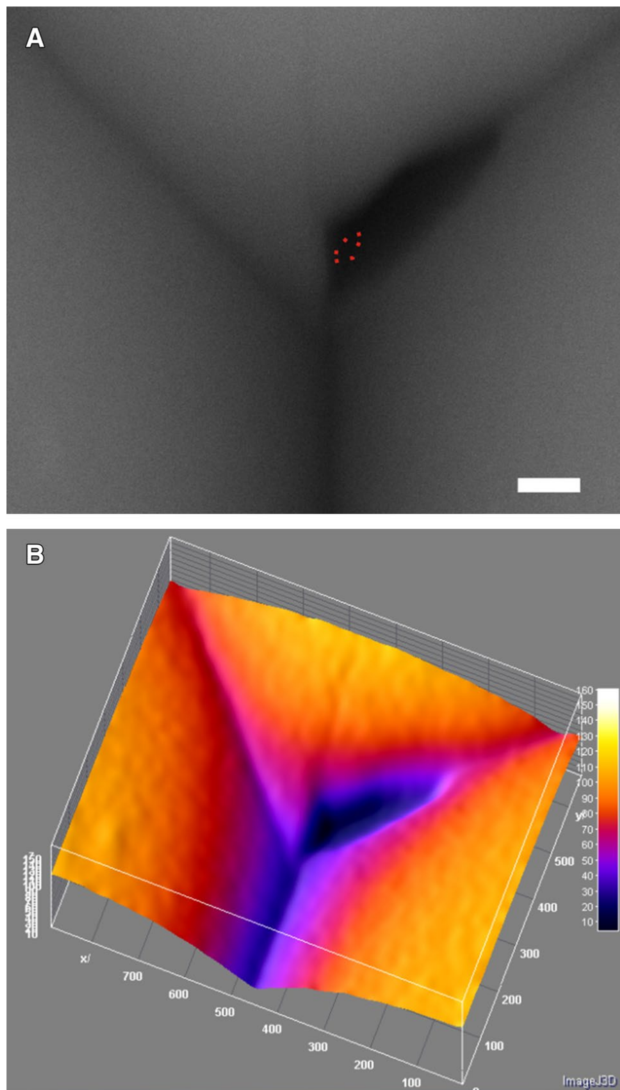

Fig. 6 **a** Nanopore SEM image obtained by etching combined with braking acid, 4 M KOH 25 °C. The *scale bar* represents 20 nm. **b** 3D image obtained from Fig. 6a with ImageJ program

was performed at 80 °C, according to Fig. 7. Since this temperature produces a higher etch rate.

The results obtained are shown in Fig. 8. In the first minute, the chemical braking is carried out at a rate of 1.23 µm/min, similar to reported rate in literature for these conditions (Jones and Jones 2003; Madou 2002). However, to reach a depth of 510 ± 2 microns, attack speed changed due to the contact of the two openings in the silicon wafer and the resulting mixture of HCl with KOH. However, due to temperature, KOH neutralization process is not completely generated and therefore the reaction of silicon attack is not stopped at time to forming a nanopore. Consequently, the result was the production of micropores. The same behavior was observed at lower temperatures up to 60 °C. Thus, the etching continued, but only in areas where the KOH was not neutralized.

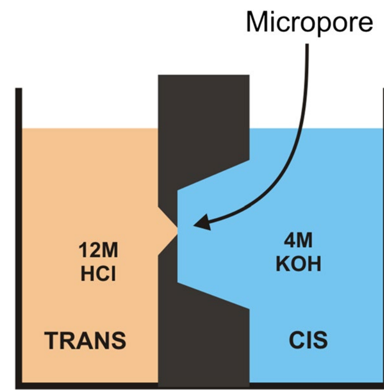

Fig. 7 Silicon micropores manufacture with chemical braking at 80 °C

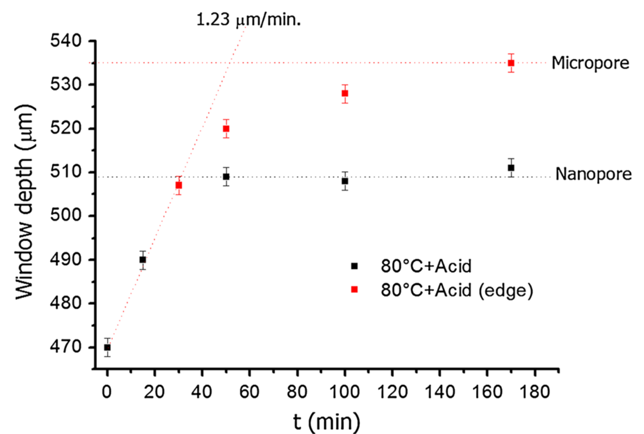

Fig. 8 Window depth of 2.1 mm, depending on the etching time with 4 M KOH at 80 °C

Figure 9 shows an image of a window marking the formation of a micropore. The light gray areas show where the etching was stopped and have a height of 510 ± 2 µm, while in external corner areas the etching continued until they reached 535 ± 2 µm depth.

3.3.3 Nanopores formation at 80 °C/potential 12

Since at the extreme condition temperature of 80 °C, the HCl do not have enough time to stop the etching with KOH in order to produce nanopores, the same etching temperature was evaluated, but applying a potential. Therefore, the potential acting as a driving force of the passage of protons to the *trans* side and thus accelerates the chemical braking to control the nanopores formation.

Nanopore formation was studied by first etching with 4 M KOH at 80 °C in the cis face and stopping the etching with 12 M HCl at 80 °C in the *trans* face. An electric potential of 12 V was applied with platinum electrodes

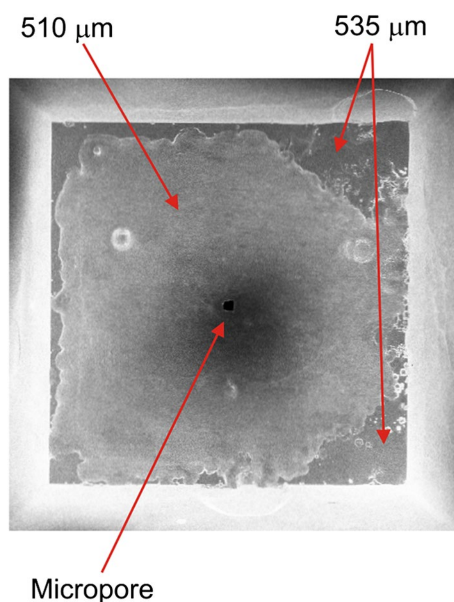

Fig. 9 SEM image of a micropore obtained by etching with 4 M KOH at 80 °C

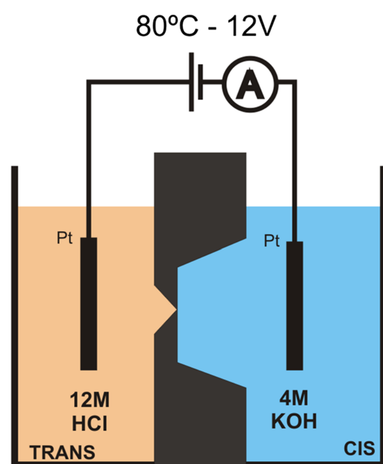

Fig. 10 Silicon nanopores fabrication with chemical braking at 80 °C/12 V

between the two compartments, placing the negative electrode on the cis face and the positive electrode in the *trans* face, according to Fig. 10. Etching continued until the two inverted pyramids found each other, and then KOH was neutralized by HCl, automatically stopping the etching forming the nanopore.

In Fig. 11 the depth measurements of the window of 2.1 mm width at different etching times on the above conditions are observed. The etching is carried out at a rate of 0.87 µm/min until the window depth reached 512 ± 2 µm, where it is deep enough for the two cavities forming the

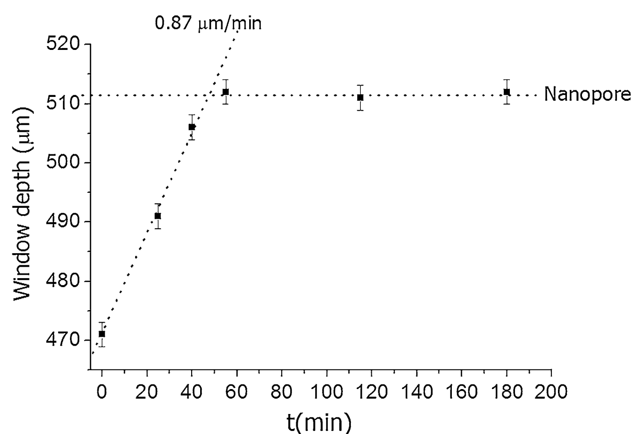

Fig. 11 Window depth of 2.1 mm, depending on the etching time, 4 M KOH at 80 °C, applying a potential of 12 V

nanopore. Once nanopore is formed, the etching stops completely. This is proven in the successive depth measurements, which do not change even when the etching is maintained until 270 min. On the other hand it can be said that if the etching had continued at the rate of 0.87 µm/min, it was observed in the initial time of nanopore formation, in 270 min window depth reached 700 µm, thus generating a millimeter cavity from side to side of the silicon wafer, instead of a nanopore, as was observed in this case.

Depth measurements were estimated by difference in height using an optical microscope. The method is reproducible and very useful when several checking steps are needed during the same etching. Additionally, this method provides a fast and easy way to identify nanopores during the manufacturing process. Figure 12a shows a nanopore formed after 60 min of chemical braking while Fig. 12b shows the same wafer after 270 min of chemical braking. It can be observed that the intensity and size of the light generated by the nanopore does not change even after a prolonged period of etching.

Silicon is a material having photo-luminescent properties in the visible light range. So that the red square that show in Fig. 12, is due to this phenomenon and is not for the light through the wafer (Cheylan et al. 2006). Red color represents only just a few pixels of the image, but can be distinguished from false positive pixels, and the red dot is located right in the area that matches the inverted pyramid formed on the opposite side of the silicon wafer. Additionally, these red dots do not appear previously to the nanopore formation and disappear when it turn off the microscope light under the silicon wafer. 3D analysis of Fig. 12a with the ImageJ program can be seen in Fig. 13, which shows the difference in light intensity corresponding to the red dot, which corresponds to the nanopore.

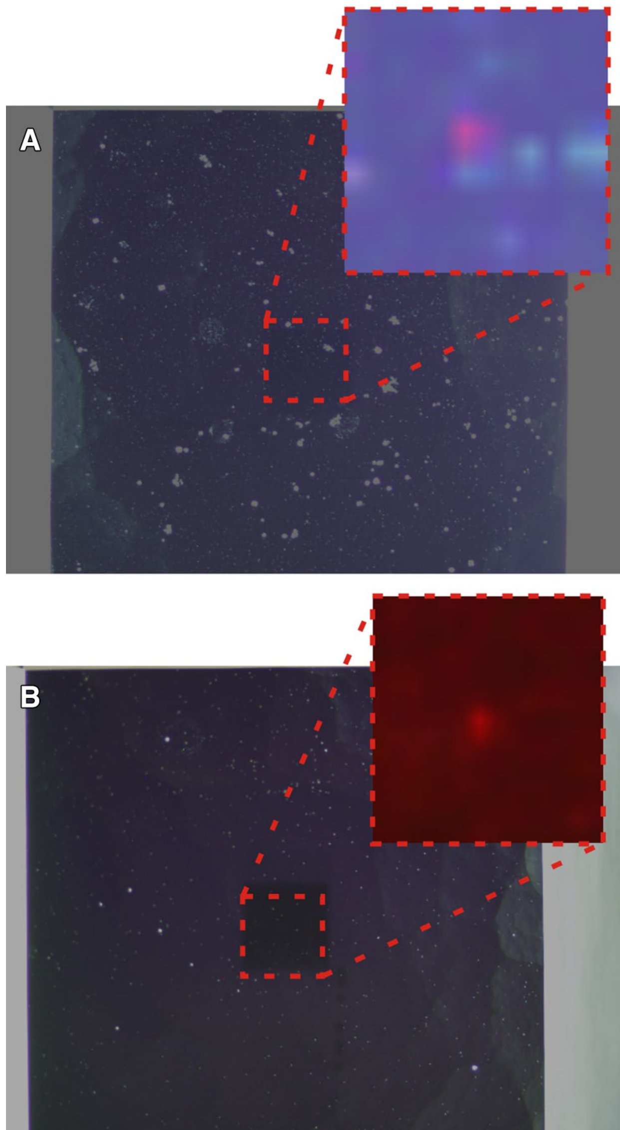

Fig. 12 **a** Nanopore identifying by optical microscopy at 60 min and **b** 270 min of etching

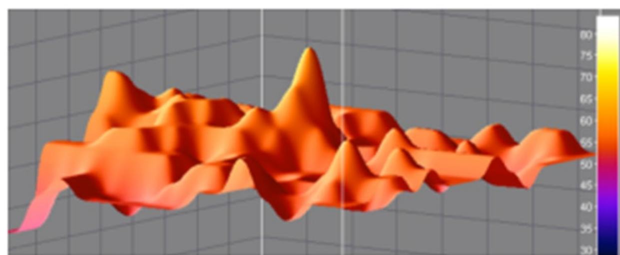

Fig. 13 3D representation of Fig. 12a

Figure 14a shows the SEM image of a nanopore, which corresponds to the same nanopore taken with an optical microscope in Fig. 12b. Analysis 3D with ImageJ program

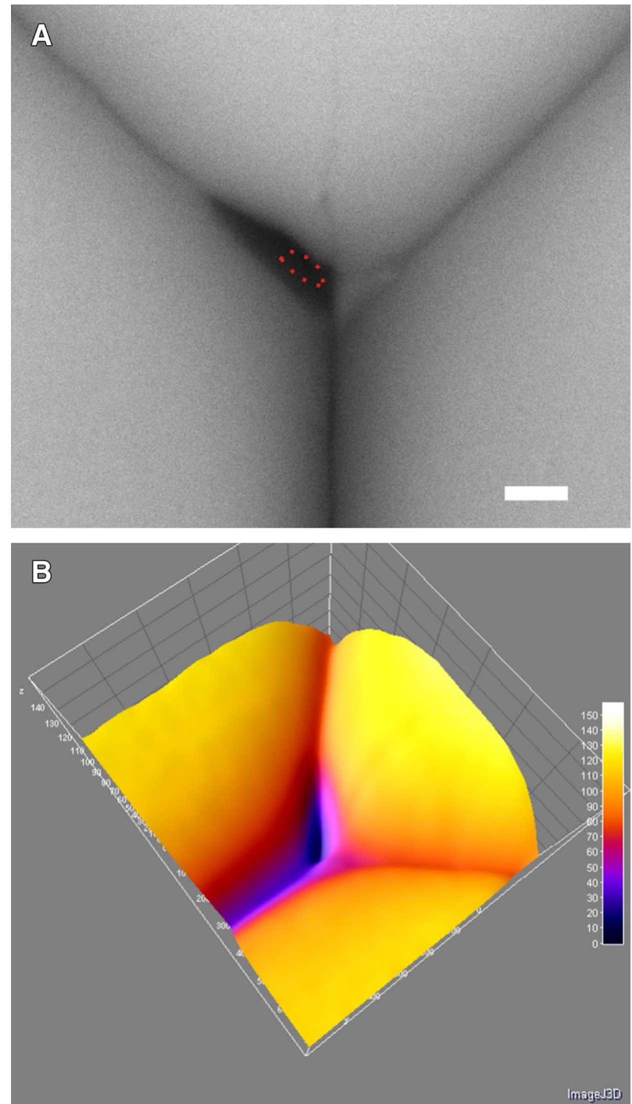

Fig. 14 **a** Nanopore SEM image obtained by acid braking method. The *scale bar* represents 20 nm. **b** 3D image obtained from Fig. 14a with ImageJ program

(Fig. 13) shows the area focused on the SEM angled walls, indicating nanopore size is less than 40 nm.

The nanopores obtained by this method are very robust compared with the other nanopores made in thin membranes, like the ones obtained by FIB (Lanyon et al. 2007; Schiedt et al. 2010) or e-beam (Rhee and Burns 2007). Our nanopores are included in a 700 µm wafer, positioned 200 µm under the wafer surface and with an inverted pyramid shape.

The advantage in the robustness becomes a problem when an image of the nanopores is desired. Because of the substrate features, it is very difficult to focus with electron microscopy (SEM or TEM), not allowing to obtain clear images at larger magnifications, preventing appreciate

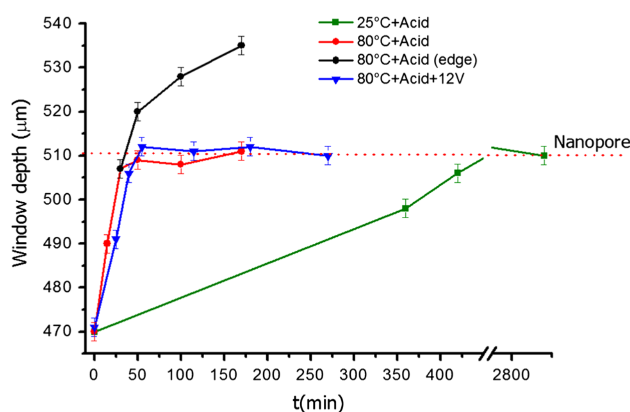

Fig. 15 Comparison of the window depth of 2.1 mm, according to the attack time for the three procedures studied

nanopore diameters below 40 nm. To overcome this problem, the characterization of the diameters was performed using resistance measurements. It is known that the diameter is related with the resistance which the nanopores presents to the ions flux (Park et al. 2007; Schneider et al. 2010; Van den Hout et al. 2010). For resistance measurements, curves I vs V was performed using 1 M KCl in both sides of the nanopore. The ion current was measured between the two sides of the silicon wafer, using Ag/AgCl electrodes. Thus, the obtained results of resistance vs diameter are compared with the results previously published by Park et al. (2007). In all cases in which nanopores were obtained, the resistance values were between 7 and 150 MΩ, indicating that the nanopore diameters obtained by this method would be between 2 and 30 nm.

The fact that the potential application when the temperature 80 °C is used stopped down the silicon etching, can be explained because the potential accelerates the protons mobility. Thus, protons traveling at faster *trans* side and stop the reaction, preventing the etching continue and ensuring the nanopores formation.

Figure 15 shows a compilation the results of the etch depth versus time for the three processes studied. In the three cases, the attachment of the two cavities produces an abrupt chemical braking for the etching. Although only in cases of chemical braking at 25 and 80 °C with the potential application it was possible obtain the nanopores. Additionally, in all cases the braking reaction occurred when a window depth of approximately 510 ± 2 μm was achieved.

The application of electric potential also had the advantage of acting as a cleaning process of the wafer surface. In cases in which the etching agent and the braking agent which can react to form salts crystallize or precipitate, applying a potential attracts ions to the electrode, leaving the substrate surface free of ions or crystals. This process is useful for industrial application, because it avoids the need for extensive subsequent washes. Figure 16 shows two wafers treated with the braking acid at 80 °C temperature. In the wafer of Fig. 16a, 12 V potential was applied and in the wafer of the Fig. 16b, potential was not applied. On the wafer on which the potential is applied, the surface was completely clean and free from reaction products. While the b wafer shows a white precipitate on the surface, corresponding to KCl that formed upon neutralization occurs.

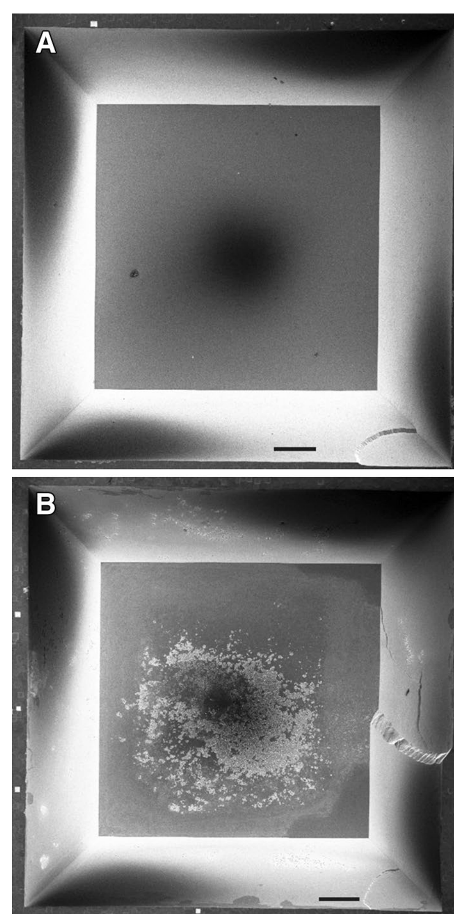

Fig. 16 Windows formed in silicon wafers etched with acid braking method. **a** With electric potential. **b** No electrical potential. The *scale bar* in both images represents 200 μm

4 Conclusions

The results presented here for the manufacture of nanopores with braking chemical method has shown several advantages over other manufacturing methods. First, the method allows to automatically stop the nanopore manufacturing process, without any feedback system or the intervention of an external agent, when this has dimensions of a few nanometers. Second, it allows to locate the nanopores in specific locations of the substrate. Third, this process has

a low cost compared to other manufacturing methods such as the FIB and e-beam. For this reason this method can be very useful for the development of new technologies for biomolecules sensing using nanopores, providing an easily adaptable methodology to mass production processes at low cost.

This paper introduces a new concept for the manufacture of nanopores, demonstrating that the proposed method works and defines a direction for future work. An extensive characterization of the method as well as the study of nanopore arrays production, will be the subject of future publications.

Acknowledgments The authors thank the financial support from CONICET-YPF (PIO-2014), ANPCyT (PICT2012-575/PICT2013-0840), and FAN 2014, Argentina. We would like to thank C. L. A. Berli, M. J. Dieguez and F. Sacco for general support and discussion.

References

Bashir BV (2011) Nanopore sensors for nucleic acid analysis. Nat Nano 6:615–624

Cheylan S, Trifonov T, Rodriguez A, Marsal L, Pallares J, Alcubilla R, Badenes G (2006) Visible light emission from macroporous. Si Optical Materials 29:262–267

Edel JB, Albrecht T (2013) Engineered nanopores for bioanalytical applications. William Andrew, New York

Fennouri A, Przybylski CD, Pastoriza-Gallego M, Bacri L, Auvray LC, Daniel RG (2012) Single molecule detection of glycosaminoglycan hyaluronic acid oligosaccharides and depolymerization enzyme activity using a protein nanopore. ACS Nano 6:9672–9678

Fologea D, Ledden B, McNabb DS, Li J (2007) Electrical characterization of protein molecules by a solid-state nanopore. Appl Phys Lett 91:053901

Gierhart BC, Howitt DG, Chen SJ, Zhu Z, Kotecki DE, Smith RL, Collins SD (2008) Nanopore with transverse nanoelectrodes for electrical characterization and sequencing of DNA. Sens Actuators B Chem 132:593–600

Hall AR, Scott A, Rotem D, Mehta KK, Bayley H, Dekker C (2010) Hybrid pore formation by directed insertion of [alpha]-haemolysin into solid-state nanopores. Nat Nanotechnol 5:874–877

Haque F, Li J, Wu H-C, Liang X-J, Guo P (2013) Solid-state and biological nanopore for real-time sensing of single chemical and sequencing of DNA. Nano Today 8:56–74. doi:10.1016/j.nantod.2012.12.008

Jones MH, Jones SH (2003) Wet-chemical etching and cleaning of silicon Fredericksburg. Va Semicond, Va

Lanyon YH, De Marzi G, Watson YE, Quinn AJ, Gleeson JP, Redmond G, Arrigan DW (2007) Fabrication of nanopore array electrodes by focused ion beam milling. Anal Chem 79:3048–3055

Lerner B, Perez M, Toro C, Lasorsa C, Rinaldi C, Boselli A, Lamagna A (2012) Generation of cavities in silicon wafers by laser ablation using silicon nitride as sacrificial layer. Appl Surf Sci 258:2914–2919

Li Y, Fan X (2013) Microring resonators with flow-through nanopores for nanoparticle counting and sizing. Opt Express 21:229–237

Madou MJ (2002) Fundamentals of microfabrication: the science of miniaturization. CRC Press, New York

Movileanu L (2008) Squeezing a single polypeptide through a nanopore. Soft Matter 4:925–931

Park SR, Peng H, Ling XS (2007) Fabrication of nanopores in silicon chips using feedback chemical etching. Small 3:116–119

Rhee M, Burns MA (2007) Nanopore sequencing technology: nanopore preparations. Trends Biotechnol 25:174–181

Rosen CB, Rodriguez-Larrea D, Bayley H (2014) Single-molecule site-specific detection of protein phosphorylation with a nanopore. Nat Biotechnol 32:179–181

Schiedt B et al (2010) Direct FIB fabrication and integration of "single nanopore devices" for the manipulation of macromolecules. Microelectron Eng 87:1300–1303

Schneider GF, Kowalczyk SW, Calado VE, Pandraud G, Zandbergen HW, Vandersypen LM, Dekker C (2010) DNA translocation through graphene nanopores. Nano Lett 10:3163–3167

Van den Hout M, Hall AR, Wu MY, Zandbergen HW, Dekker C, Dekker NH (2010) Controlling nanopore size, shape and stability. Nanotechnology 21:115304